Supporting Information

Supercritical CO_2-synthesis of Co-doped MoO_{3-x} nanocrystals for multifunctional light utilization

Xiaoli Zheng,[a,‡] Xuzhe Wang,[a,b,‡] Qingyong Tian,[a,c] Xinwei Cui,[a,*] Yannan Zhou,[a] Tianpei Ge,[a] Wei Liu,[a] Cong Wei,[a] Qun Xu[a,c,*]

1. Experimental Section

Materials.

Commercially bulk MoO_3 was purchased from Sigma Aldrich (Product Number: 267856). Cobalt(II) nitrate hexahydrate ($Co(NO_3)_2 \cdot 6H_2O$), Nickel(II) nitrate hexahydrate ($Ni(NO_3)_2 \cdot 6H_2O$), methylene blue (MB) and ethanol were purchased from Sinopharm Chemical Reagent Co., Ltd. (China). CO_2 gas with purity of 99.999% was provided by Henan Keyi gas co. LTD. All of the chemicals were used directly without further purification.

Synthesis of Co-MoO_{3-x} nanocrystals (NCs).

The Co-MoO_{3-x} NCs were synthesized according to the reported method with some modifications.[1] Typically, 100 mg of bulk MoO_3 powder was added into 10 mL of ethanol/water mixture (5:5/v:v). The mixture was continuously sonicated in an ice bath for 8 h. Then the sonicated dispersion was centrifuged at 3000 rpm for 45 minutes and the supernatant is obtained. The concentration of the MoO_3 supernatant was determined to be 2 mg mL^{-1}. Then, 10 mL of the MoO_3 supernatant was mixed with 5.4 mg (13.3% atom%) of $Co(NO_3)_2 \cdot 6H_2O$. Then the dispersion was quickly transferred into the supercritical CO_2 apparatus with a heating jacket and a temperature controller. The reactor was charged with CO_2 up to 10 MPa at 100 °C. Subsequently, the temperature was slowly elevated to 200 °C and maintained for 6 hours with magnetic stirring. Then, the reactor was cooled naturally to room temperature. After depressurization, the product was collected and centrifuged at 5000 rpm for 10 minutes, then the supernatant was taken out and dried in vacuum at 100 °C for 1 hour. The supercritical CO_2-treated MoO_3 (S-MoO_3) was prepared without the addition of $Co(NO_3)_2 \cdot 6H_2O$. Varied contents of Co-doped (1.8, 3.5 and 7.2 atom %) MoO_{3-x} NCs were also prepared with the same procedure but with different additive amount of $Co(NO_3)_2 \cdot 6H_2O$ (0.73 mg, 1.41 mg and 2.90 mg, respectively). The control experiment was also conducted by the same procedure as that of Co-MoO_{3-x} NCs but without the SC CO_2.

Characterization.

The morphology and structure of the materials was characterized by Field-emission scanning electron microscope (FE-SEM, JSM7500F) and transmission electron microscopy (TEM) (JEM-2100). X-ray diffraction (XRD) patterns of samples were measured on a Netherlands X′Pert PRO X-ray diffractometer with copper Kα radiation (λ =1.5406 Å). X-ray photoelectron spectroscopy was performed using Thermo ESCLAB 280 system. Inductively coupled plasma atomic emission spectroscopy (ICP-AES) was performed using ICPE-9820213DF0G. The ICP-AES is performed to characterize the concentration of metal elements by quantifying the metal spectral signatures in nitric acid-digested samples. Then the atomic ratio of Mo/Co are calculated from the concentration of the Mo and Co elements gained from the ICP-AES data. Raman measurements were carried out on a Renishaw microscope System RM 2000. UV/Vis-NIR absorption spectra was measured by using a U-4100 UV/Vis-NIR spectrometer (Hitachi).

Raman Measurement.

Raman spectra of MB deposited on the as-prepared samples as substrates were characterized under laser excitation at 632 nm. 1 mL of MB solution with given concentration was mixed with 500 μL of sample dispersion (1 mg mL^{-1}) followed by 2 h storage in dark for an adsorption equilibrium. Finally, 20 μL suspension was extracted and dropped onto a cleaned silicon wafer (3 mm × 3 mm) followed by drying at 60 °C. Raman spectra of all samples were measured under same conditions afterward. Raman measurement parameters setting: laser wavelength: 632 nm; power: 0.5 mW; lens: 50 × long distance objective; acquisition: 10 s.

The Calculation Equation of Enhancement Factor (EF).

The Raman signal data for MB (10^{-2} M) is used as non-SERS-active reference. Specifically, the intensity was obtained by taking average from measurements of several spots, and the EF was calculated as the following equation:[2,3]

$$\mathrm{EF} = (I_{SERS}/I_{Bulk})(N_{Bulk}/N_{SERS}) \qquad (1)$$

$$\mathrm{N} = \mathrm{CV}N_A S_{Raman}/S_{sub} \qquad (2)$$

Where I_{SERS} is the Raman intensity of MB on the SERS-active substrate and I_{Bulk} is the intensity of the same Raman band under non-SERS conditions, used as reference. A 10^{-2} M MB solution was employed as the reference. N_{SERS} is the number of MB molecules absorbed on the SERS-active substrate under the laser spot area and N_{Bulk} is the number of molecules illuminated within the volume of the laser waist for the MB bulk solution. C is the molar concentration of the probe molecule solution, V is the volume of the droplet, N_A is Avogadro constant. S_{Raman} is the laser spot area (1 μm in diameter) of Raman scanning, and S_{Sub} is the area of the substrate (3 mm × 3 mm). This equation is based on the assumption that the probe molecules were distributed uniformly on the substrates.

Photothermal measurements.

For evaluating the photothermal conversion efficiency of Co-MoO_{3-x} NCs, at first the Co-MoO_{3-x} NCs can be dispersed well in deionized water by ultrasonication to obtain dispersion with different concentrations (50-1000 μg ml^{-1}), and the absorption at 808 nm wavelength of the all dispersion were determined by using UV/vis-NIR spectrophotometer. Then 1 mL aqueous dispersion of Co-MoO_{3-x} were moved into a small glass bottle with 1.5 mL volume, and irradiated under an 808 nm NIR laser at the power density of 1.06 W cm^{-2}. The temperature of the dispersion was real-time measured every 30 s after the start of irradiation via thermocouple temperature probe. After the NIR laser irradiation was shut off, the cooled temperature data was recorded for about 1200 s with the same intervals. In order to investigate the stability of dispersion, six irradiation cycles were conducted under a repeated procedure with laser on and then laser-off versus time. Pure water and other samples were measured under the same conditions. Photothermal conversion efficiency (η) of Co-MoO_{3-x} NCs was calculated according to the Roper's method.[4]

Calculation of the photothermal conversion efficiency (η)**.**

The photothermal conversion efficiency (η) can be calculated by Eq (1).[4,5]

$$\eta = \frac{hA(\Delta T_{max} - \Delta T_{max,H_2O})}{I(1 - 10^{-A_\lambda})} \qquad (1)$$

Where h is the heat transfer coefficient, A is the surface area of the container, ΔT_{max} and $\Delta T_{max,H2O}$ are the temperature change of the sample dispersion and deionized water at the maximum steady-state temperature, respectively. *I* is the 808 nm NIR laser power, and A_λ is the absorbance at 808 nm wavelength. In this equation, only hA is unknown. So θ is introduced, which is defined as the ratio of ΔT to ΔT_{max} (Eq (2)).

$$\theta = \frac{\Delta T}{\Delta T_{max}} \qquad (2)$$

In addition, the total energy balance of this system can be calculated by Eq (3).

$$\sum_i m_i C_{p,i} \frac{dT}{dt} = Q_A + Q_H - Q_{loss} \qquad (3)$$

Where m and C_p are the mass and heat capacity, respectively. The suffix "i" of m and C_p refers to solvent (water) and dispersed matter. T is the solution temperature. Q_A is the photothermal energy absorbed by sample dispersion per second. Q_H is the heat associated with the light absorbed by water solvent per second. Q_{loss} is the thermal energy lost to the surroundings. When the laser was shut off, the $Q_A + Q_H = 0$. Substituting equation (2) into equation (3) can obtain Eq (4).

$$t = -\frac{\sum_i m_i C_{p,i}}{hA} \ln\theta \qquad (4)$$

where $\tau_s = \frac{\sum_i m_i C_{p,i}}{hA}$ can be calculated by linear relationship of time versus – lnθ, τ_s is the time constant for heat transfer. Owing to the mass of the samples (1×10^{-6} Kg) is far less than that of water solvent (1×10^{-3} Kg), and the specific heat of water is much higher than other materials. Therefore, the m_i and $C_{p,i}$ of the samples are neglected. m_{H2O} is 1×10^{-3} Kg, $C_{p,H2O}$ is 4.2×10^{3} J $Kg^{-1}°C^{-1}$. So hA value can be got in this way, and the η of samples could be calculated.

2. Supplemental Figures and Tables

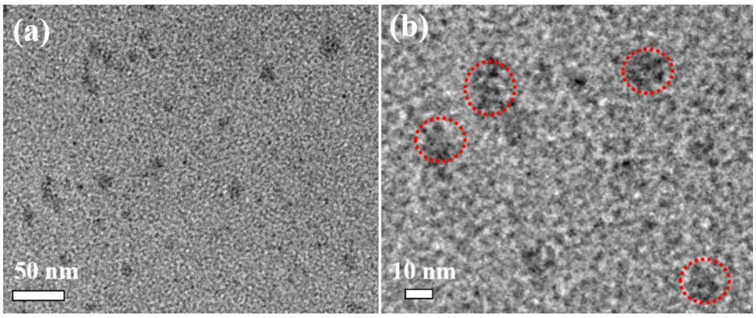

Figure S1. (a, b) TEM images of Ni_xMoO_3 amorphous nanodots with average size of 16.0 nm.

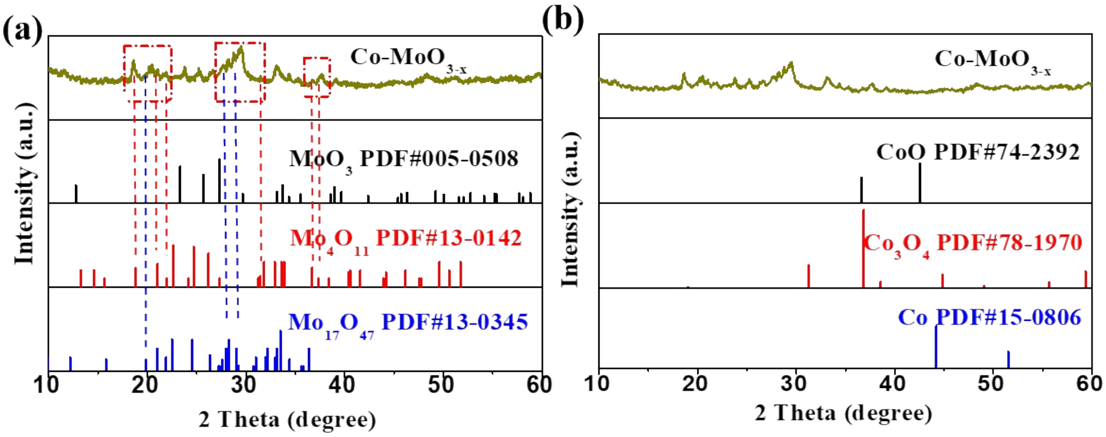

Figure S2. (a) XRD patterns for Co-MoO_{3-x}, MoO_3 (PDF#005-0508), Mo_4O_{11} (PDF#13-0142) and $Mo_{17}O_{47}$ (PDF#13-0345). (b) XRD patterns for Co-MoO_{3-x}, CoO (PDF#74-2392), Co_3O_4 (PDF#78-1970), and Co (PDF#15-0806).

As shown in Figure 1a and Figure S2a, some extra peaks marked by the red dotted rectangles in the Co-MoO_{3-x} NCs can be well assigned to the orthorhombic $Mo_{17}O_{47}$, JCPDS No. 13-0345 (20.1°-(240), 27.7°-(231), 28.3°-(630), 28.8°-(041), 29.4°-(141)) and monoclinic Mo_4O_{11}, JCPDS No. 13-0142 (18.7°-(-401), 21.0°-(011), 21.9°-(-211), 31.6°-(112), 37.5°-(-612)), respectively, implying that oxygen vacancy are introduced during the synthesis procedure. Moreover, the relevant Co and Co oxide database patterns of Co (PDF#15-0806), CoO (PDF#74-2392) and Co_3O_4 (PDF#78-1970) shown in Figure S2b confirm that there is no separate Co or Co oxide phases formed in the Co-MoO_{3-x} NCs, suggesting a homogeneous distribution of the Co-doping. This XRD analysis reveals that our as-synthesized materials are Co-incorporated, sub-stoichiometric MoO_{3-x}.

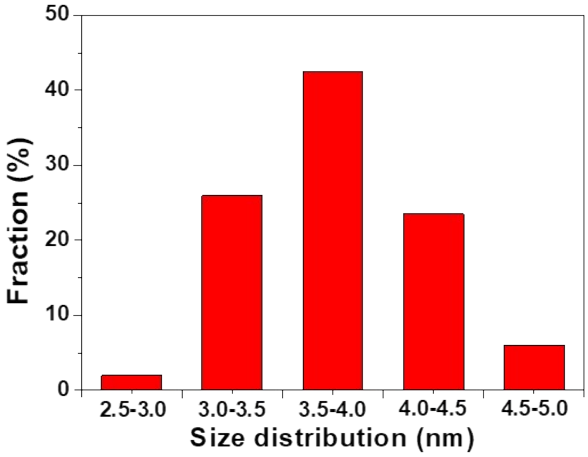

Figure S3. The statistical analysis of the lateral sizes of Co-MoO_{3-x} NCs.

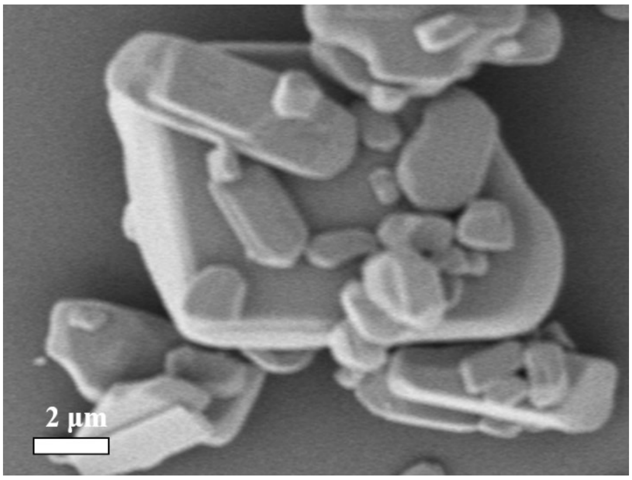

Figure S4. SEM image of B-MoO_3.

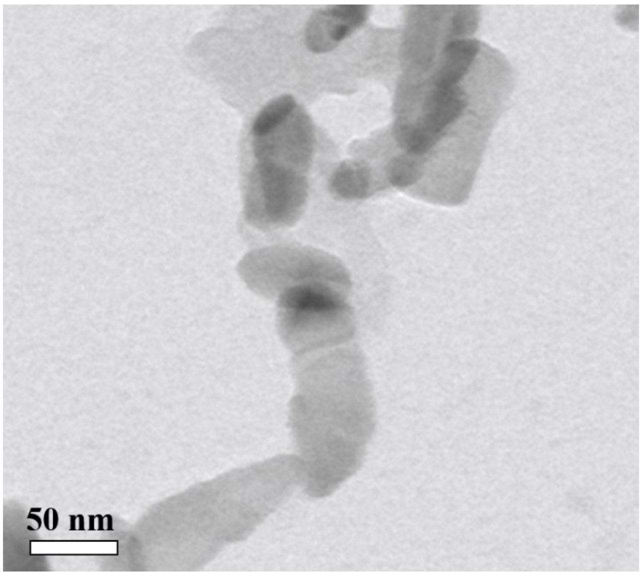

Figure S5. TEM image of the S-MoO_3.

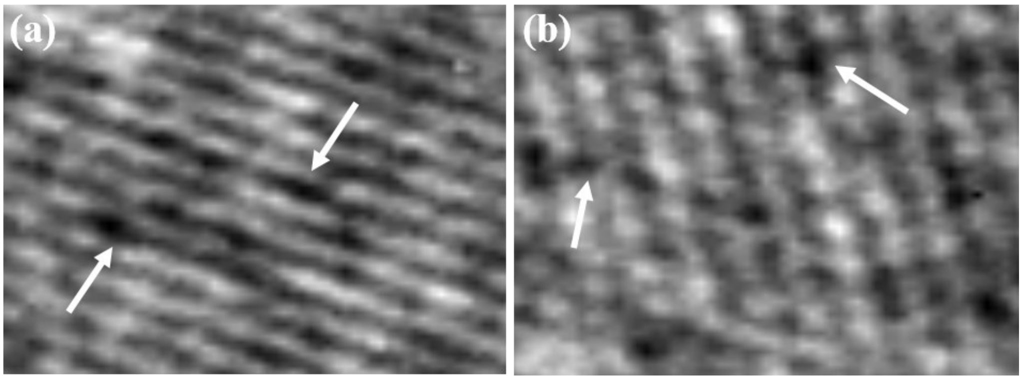

Figure S6. The inversed FFT images of Fig. b1 and Fig. b2, respectively. As shown in Figure S6, there are vast defects in the matrix of NCs (indicated by arrows).

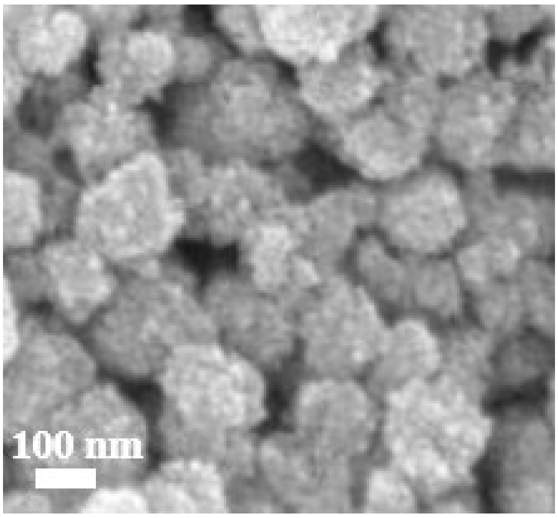

Figure S7. SEM image of the Co-doped MoO_3 without the supercritical CO_2.

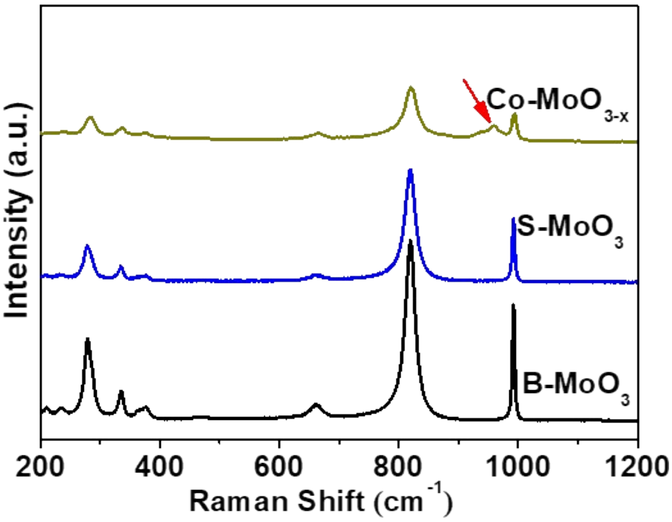

Figure S8. Raman spectra of Co-MoO_{3-x}, S-MoO_3 and B-MoO_3.

The Raman spectra of the samples were obtained to investigate the band structure of the samples. As shown in Fig. S8, after the incorporation of Co, a new peak appears at 957.2 cm^{-1}, representing the Mo=O stretching vibrational mode in the sub-stoichiometric MoO_{3-x}. Overall, these characterization results demonstrate that the incorporation of Co ions with the assistance of SC CO_2 can successfully create a high level of Co doping, and a large number of penta-coordinated Mo^{5+} and O_V, forming Co-MoO_{3-x} NCs.

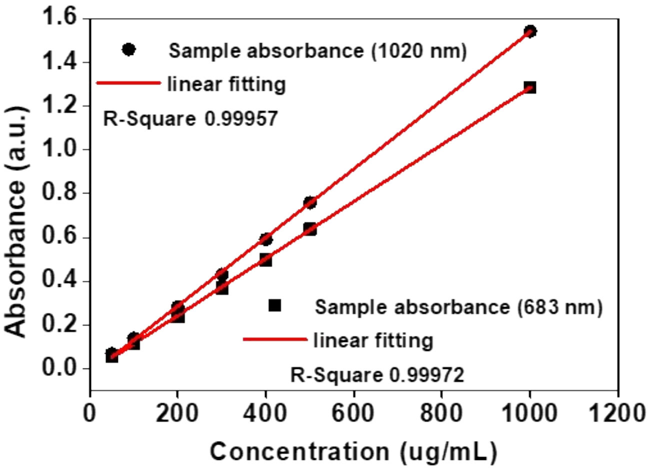

Figure S9. Linear fitting of sample absorbance at 683 nm and 1020 nm versus the weight concentrations of the Co-MoO_{3-x} NCs.

The absorption intensity at the 683 and 1020 nm are fitted *versus* the Co-MoO_{3-x} concentrations, wherein the good linear relationship indicates that the Co-MoO_{3-x} NCs are well dispersed in water.

The molar extinction coefficient (ε) of these Co-MoO_{3-x} NCs was determined by measuring the extinction spectra of seven different Co-MoO_{3-x} NC solutions, applying the Lambert-Beer law.[6]

$$A(\lambda) = \varepsilon \times b \times c$$

where A is the absorbance at a given wavelength λ, ε is the molar extinction coefficient in M^{-1} cm^{-1}, b is the optical path length in cm (0.3 cm in this case) and c is the molar concentration of the NCs. NC concentrations were determined from their weight concentration shown in Figure S8, taking into account the volume of a single NC, and the volume and the stoichiometry of the unit cell. For convenience, the unit cell NC is considered to be MoO_3. From the slope of the linear fit of each curve, the ε

value can be obtained by dividing the slope with the path length: $\varepsilon = 3.8 \times 10^5$ M^{-1} cm^{-1} at 683 nm and 4.6×10^5 M^{-1} cm^{-1} at 1020 nm.

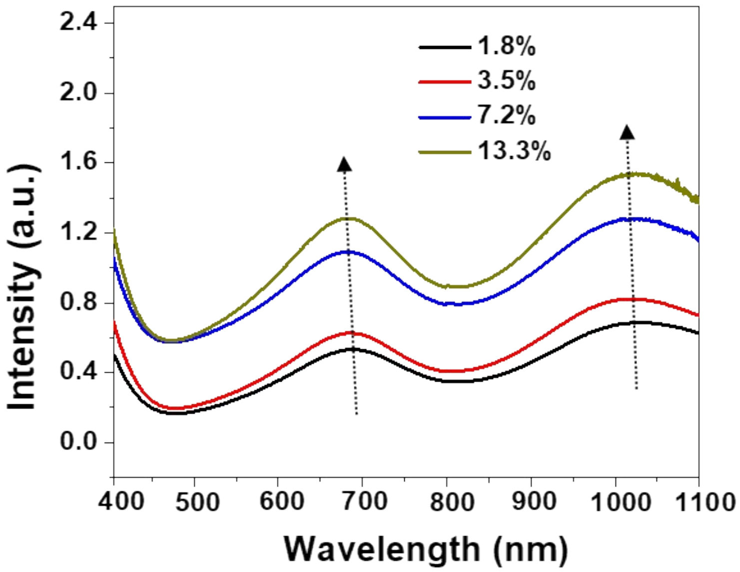

Figure S10. UV/vis-NIR absorbance spectra from solutions of 1.8, 3.5 7.2, and 13.3 atom % of Co-doped MoO_{3-x} NCs, all at the same concentration by mass (1 mg mL^{-1}).

As shown in Figure S10, all the Co-MoO_{3-x} NCs prepared with different atoms% of Co-doing show remarkably absorption peaks in the vis-NIR region. The intensity of these absorption peaks gradually increase and the peak frequency undergoes blue shift with an increase of the Co-dopant concentration, signifying the donor behavior of Co-dopant and the resultant LSPR response.

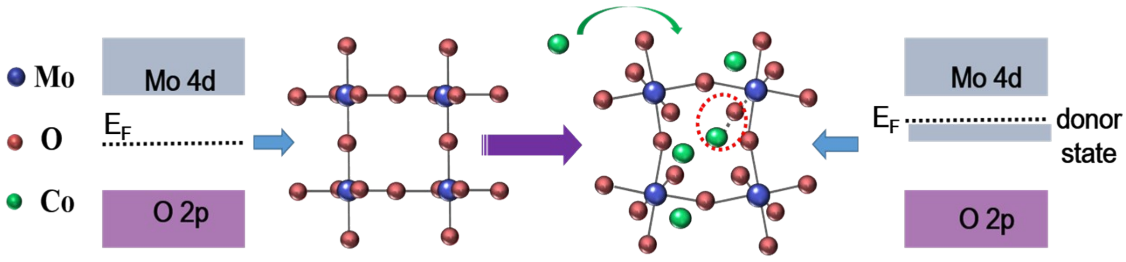

Figure S11. Simplified crystal structures of MoO_3 and Co-MoO_{3-x}. The electronic structures of the MoO_3 and Co-MoO_{3-x} are depicted in the left and right panel, respectively.

From the work function theory, the abundant oxygen vacancies and Co-doping generate donor state, which contribute significantly increased free electron carriers, leading to strong LSPR response in the vis-NIR regions.

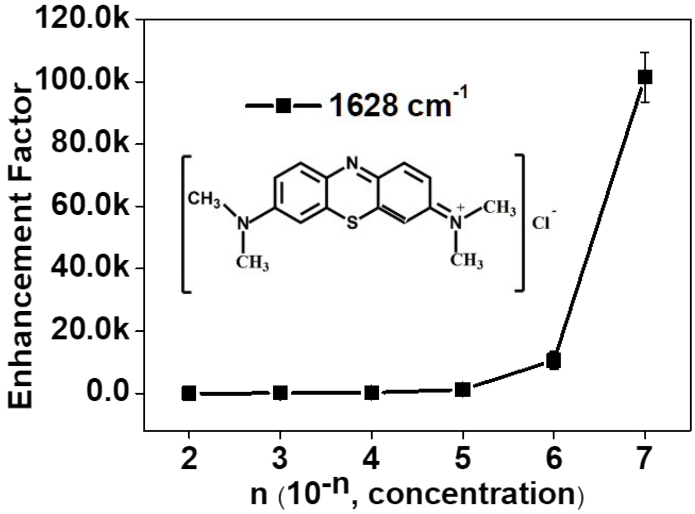

Figure S12. The enhancement factor (EF) of the SERS sensor at 1628 cm^{-1} peak as a function of MB concentration. The Raman signals at each concentration are measured from 3 points to ensure the accuracy of the results.

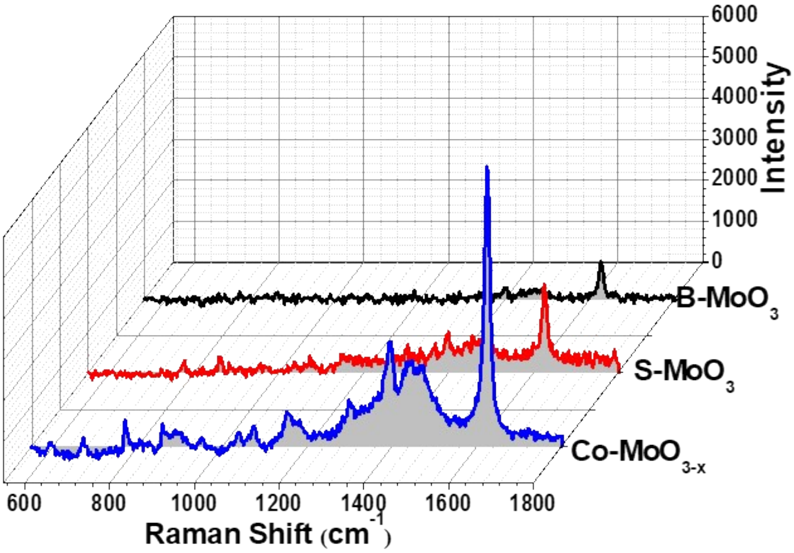

Figure S13. Raman spectra of MB (10^{-2} M) on the Co-MoO_{3-x}, S-MoO_3 and B-MoO_3 SERS substrates. Obviously, the Co-MoO_{3-x} exhibits the largest enhancement, and the SERS intensity at 1628 cm^{-1} is about 7.4 and 3.2 times larger than that of B-MoO_3 and S-MoO_3, respectively.

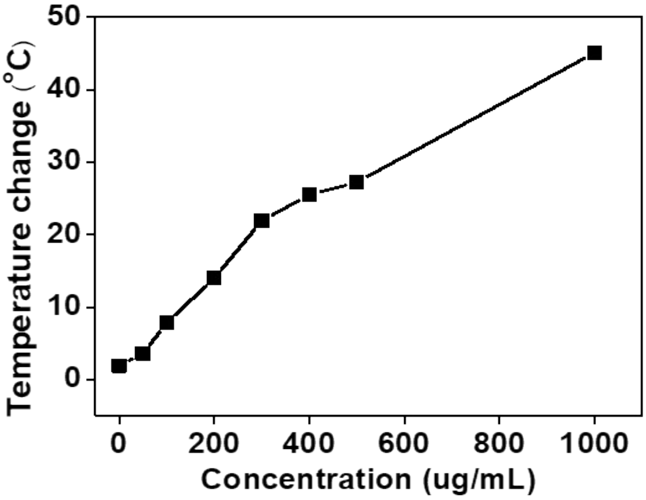

Figure S14. Plot of temperature variation upon a 480 s irradiation versus the concentrations of the Co-MoO_{3-x} NCs.

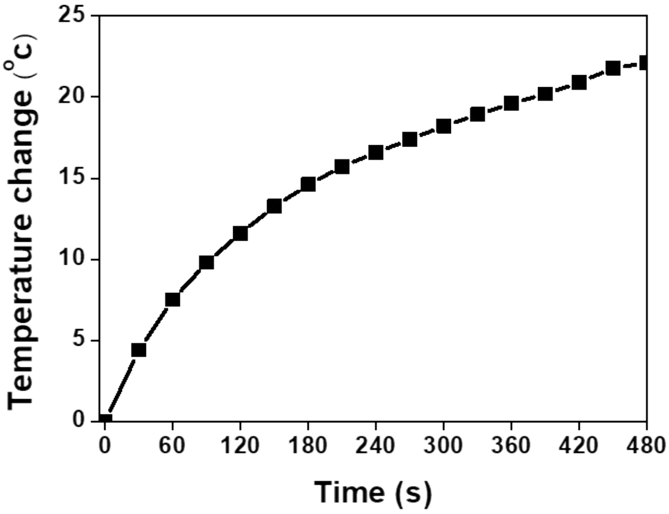

Figure S15. Temperature changes of the S-MoO_3 suspension as a function of irradiation duration.

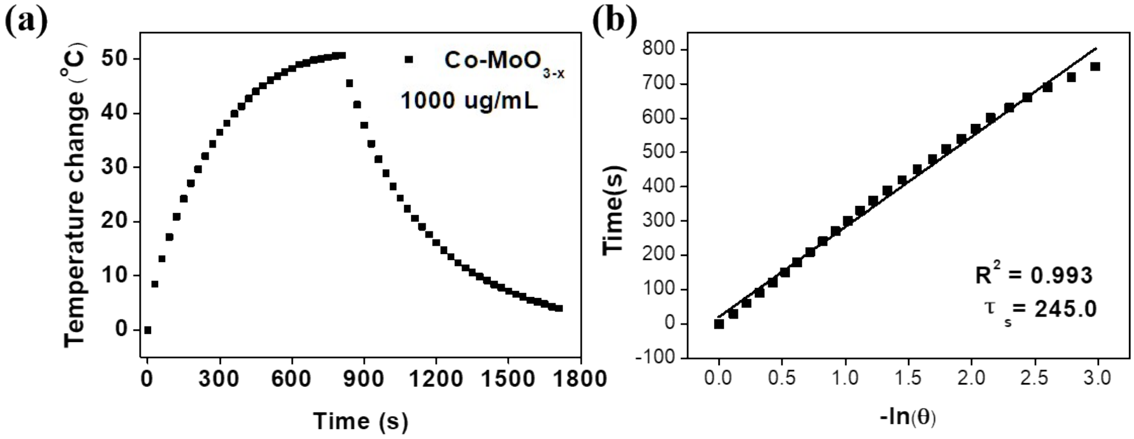

Figure S16. (a) Photothermal response of the Co-MoO_{3-x} NCs (1000 μg mL^{-1}) versus time with laser-on and then laser-off. (b) Plot of the cooling time versus the negative natural logarithm of the temperature driving force, deduced from the cooling section of (a). Time constant for heat transfer from the system is determined to be $\tau_s = 245.0$ s.

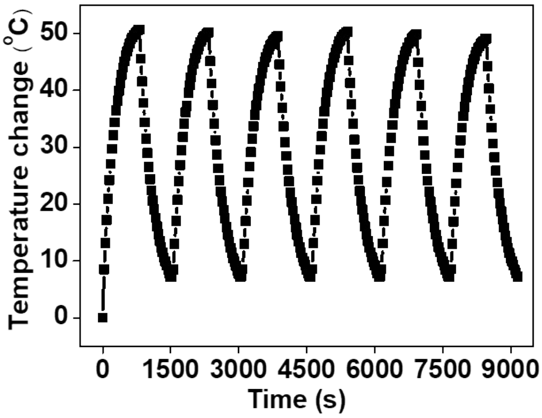

Figure S17. Temperature changes of the Co-MoO_{3-x} NCs (1000 μg/mL) over 6 irradiation cycles.

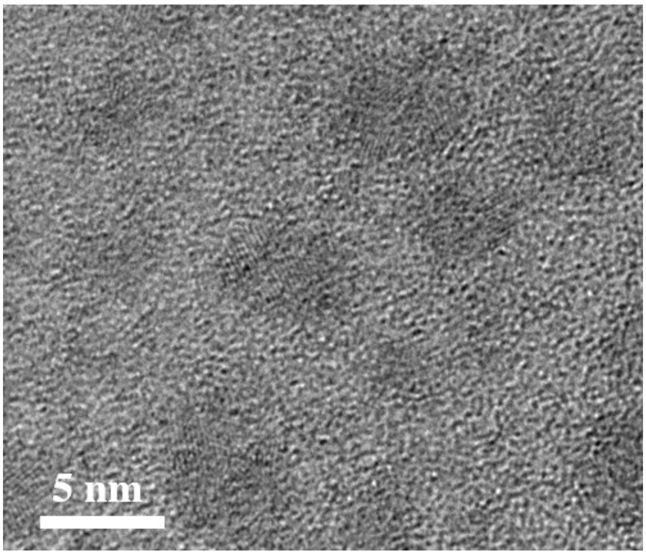

Figure S18. HRTEM image of the Co-MoO_{3-x} NCs after the photothermal conversion test.

Table S1. SERS property comparison with previous works.

Substrate	Detection sensitivity (M)	EF	Molecules	References
MoO_2 nanosheet	10^{-7}	___	MB	*J. Mater. Chem. C* 2019, **7**, 7196[7]
Ag NPs microfluidic system	10^{-7}	___	MB	*Sci. Rep.* 2019, **9**,17634[8]
Ag NPs/3D graphene foam	10^{-6}	5×10^4	MB	*Sci. Rep.* 2016, **6**, 23733[9]
MoO_{3-x}@ MoO_3	10^{-7}	1.42×10^5	MB	*Chem. Commun.* 2016, **52**, 2893[10]
Co-MoO_{3-x} NCs	10^{-7}	1.01×10^5	MB	This work

Table S2. Photothermal conversion property comparison with previous works.

Samples	Photothermal conversion efficiency (PCE)	incident laser power	References
core–shell TiO_2 nanoparticles	55.2%	1.0 W/cm^2 (808 nm)	*Nanoscale* 2017, 9, 16183[11]
Au-Cu_9S_5 NPs	37%	0.7 W/cm^2 (1064 nm)	*J. Am. Chem. Soc.* 2014, 136, 15684[12]
$Ti_xTa_{1-x}S_yO_z$ nanosheets	39.2%	1.0 W/cm^2 (808 nm)	*Angew. Chem. Int. Ed.* 2017, 56, 7842[13]
partial crystallized 2D VO_2	78.8%	1.06 W/cm^2 (808 nm)	*Angew. Chem. Int. Ed.* 2020, 59, 3322[14]
Amorphous MoO_{3-x} nanosheets	61.79%	1.06 W/cm^2 (808 nm)	*Chem. Commun.* 2019, 55, 12527[5]
Co-MoO_{3-x} NCs	80.1%	1.06 W/cm^2 (808 nm)	This work

References

1 X. Wang, P. Yan, Q. Xu, H. Li, C. Guo and C. Liu, *Chem. Commun.*, 2019, **55**, 9777-9780.

2 H. Li, Q. Xu, X. Wang and W. Liu, *Small*, 2018, **14**, 1801523.

3 J. Li, W. Zhang, H. Lei and B. Li, *Nano Res.,* 2018, **11**, 2181-2189.

4 D. K. Roper, W. Ahn and M. Hoepfner, *J. Phys. Chem. C,* 2007, **111**, 3636-3641.

5 C. Guo, P. Yan, C. Zhu, C. Wei, W. Liu, W. Wu, X. Wang, L. Zheng, J. Wang, Y. Du, J. Chen and Q. Xu, *Chem. Commun.,* 2019, **55**, 12527-12530.

6 S. Ghosh, T. Avellini, A. Petrelli, I. Kriegel, R. Gaspari, G. Almeida, G. Bertoni, A. Cavalli, F. Scotognella, T. Pellegrino and L. Manna, *Chem. Mater.*, 2016, **28**, 4848-4858

7 X. Lin, P. Yan, F. Xu, W. Wu, T. Hu, C. Wei and Q. Xu, *J. Mater. Chem. C,* 2019, **7**, 7196-7200.

8 X. Zhang, H. Zhang, S. Yan, Z. Zeng, A. Huang, A. Liu, Y. Yuan and Y. Huang, *Sci. Rep.,* 2019, **9**, 17634.

9 C. Srichan, M. Ekpanyapong, M. Horprathum, P. Eiamchai, N. Nuntawong, D. Phok-haratkul, P. Danvirutai, E. Bohez, A. Wisitsoraat and A. Tuantranont, *Sci. Rep.,* 2016, **6**, 23733.

10 X. Tan, L. Wang, C. Cheng, X. Yan, B. Shen and J. Zhang, *Chem. Commun.,* 2016, **52**, 2893-2896.

11 L. Sun, Z. Li, Z. Li, Y. Hu, C. Chen, C. Yang, B. Du, Y. Sun, F. Besenbacher and M. Yu, *Nanoscale,* 2017, **9**, 16183-16192.

12 X. Ding, C. H. Liow, M. Zhang, R. Huang, C. Li, H. Shen, M. Liu, Y. Zou, N. Gao, Z. Zhang, Y. Li, Q. Wang, S. Li and J. Jiang, *J. Am. Chem. Soc.,* 2014, **136**, 15684-15693.

13 C. Tan, L. Zhao, P. Yu, Y. Huang, B. Chen, Z. Lai, X. Qi, M. H. Goh, X. Zhang, S. Han, X.-J. Wu, Z. Liu, Y. Zhao and H. Zhang, *Angew. Chem. Int. Ed.,* 2017, **56**, 7842-7846.

14 Y. Zhou, Q. Xu, T. Ge, X. Zheng, L. Zhang and P. Yan, *Angew. Chem. Int. Ed.,* 2020, **59**, 3322-3328